Journal of the Brazilian Society of Mechanical Sciences and Engineering (2018) 40:449
https://doi.org/10.1007/s40430-018-1360-9

TECHNICAL PAPER

Three-dimensional unsteady flow of Maxwell fluid with homogeneous–heterogeneous reactions and Cattaneo–Christov heat flux

Maria Imtiaz[1] · Asmara Kiran[2] · Tasawar Hayat[2,3] · Ahmed Alsaedi[3]

Received: 22 March 2018 / Accepted: 13 August 2018 / Published online: 27 August 2018

Abstract

This article addresses the unsteady three-dimensional flow of Maxwell fluid. Flow is induced by a bidirectional stretching surface. Fluid fills the porous space. Thermal relaxation time is examined using Cattaneo–Christov heat flux. Homogeneous–heterogeneous reactions are also considered. Suitable transformations are used to convert partial differential equations into nonlinear ordinary differential equations. Convergent series solutions are obtained. Effects of appropriate parameters on the velocity, temperature and concentration fields are examined. It is found that increasing value of Deborah number decreases the fluid flow. Larger values of strength of homogeneous reaction parameter decrease the concentration distribution. Also temperature is decreasing function of thermal relaxation time. Present problem is of great interest in biomedical, industrial and engineering applications like food processing, clay coatings, hydrometallurgical industry, fog formation and dispersion.

Keywords Unsteady flow · Maxwell fluid · Cattaneo–Christov heat flux · Porous medium · Homogeneous–heterogeneous reactions

List of symbols

u, v, w	Velocity components along x-, y- and z-axes, respectively ($\mathrm{ms^{-1}}$)
T	Temperature (K)
T_w	Surface temperature (K)
T_∞	Ambient fluid temperature (K)
k_c, k_s	Rate constant
A, B	Chemical species
k	Thermal conductivity ($\mathrm{WK^{-1}\ m^{-1}}$)
$\hat{k}$	Permeability ($\mathrm{m^2}$)
c, d	Stretching constants ($\mathrm{s^{-1}}$)
a, b	Concentrations of the species A and B
$\mathbf{q}$	Specific heat flux
a_0	Positive dimensional constant
C_p	Specific heat ($\mathrm{m^2\ s^{-2}}$)
C_{fx}, C_{fy}	Local skin friction coefficient along x- and y-axes, respectively
D_A, D_B	Diffusion species coefficients
Pr	Prandtl number
u_w	Stretching sheet velocity along x-axis ($\mathrm{ms^{-1}}$)
v_w	Stretching sheet velocity along y-axis ($\mathrm{ms^{-1}}$)
Re_x, Re_y	Local Reynolds number
A_1	Unsteady parameter
Sc	Schmidt number
K	Strength of the homogeneous reaction
K_1	Strength of the heterogeneous reaction

Greek symbols

μ	Viscosity ($\mathrm{kg\ m^{-2}\ s^{-1}}$)
υ	Kinematic viscosity ($\mathrm{m^2\ s^{-1}}$)
ρ	Density ($\mathrm{kg\ m^{-3}}$)
λ_1	Heat flux relaxation time
λ	Retardation time
θ	Dimensionless temperature

Technical Editor: Cezar Negrao.

✉ Maria Imtiaz
mi_qau@yahoo.com

[1] Department of Mathematics, University of Wah, Wah Cantt 47040, Pakistan

[2] Department of Mathematics, Quaid-I-Azam University 45320, Islamabad 44000, Pakistan

[3] Nonlinear Analysis and Applied Mathematics (NAAM) Research Group, Department of Mathematics, Faculty of Science, King Abdulaziz University, Jeddah 21589, Saudi Arabia

ξ	Transformed coordinate
α	Time constant (s^{-1})
k_1	Porosity parameter
β_1	Deborah number
τ_{wx}, τ_{wy}	Wall shear stress
γ	Thermal relaxation parameter
β_2	Ratio of stretching rates
δ	Ratio of diffusion coefficient

1 Introduction

At present researchers and engineers are giving special attention to the study of non-Newtonian fluid. These fluids have various applications in polymer solutions, paints, certain oils, food items, salt solutions, clay coatings, cosmetic products, etc. Non-Newtonian fluids are divided into three categories as the differential, the rate and the integral types. Rate-type fluids describe the behavior of relaxation time and retardation time. Maxwell fluid is simplest subclass of rate-type fluid. Maxwell fluid describes the characteristics of relaxation time. Sui et al. [1] studied slip flow of Maxwell nanofluid with Cattaneo–Christov double-diffusion induced by a stretching sheet. Helical flows of Maxwell fluid between coaxial cylinders have been discussed by Jamil and Fetecau [2]. Wang and Tan [3] studied stability analysis of soret-driven double-diffusive convection of Maxwell fluid in a porous medium. Abbasbandy et al. [4] analyzed Falkner–Skan flow of MHD Maxwell fluid. Three-dimensional boundary layer flow of Maxwell fluid is studied by Awais et al. [5]. Stretched flow of Maxwell fluid with heat source/sink is studied by Ramesh and Gireesha [6]. Ramesh et al. [7] examined three-dimensional flow of Maxwell fluid with suspended nanoparticles past a porous stretching surface with thermal radiation. Stagnation point flow of Maxwell fluid toward a permeable surface in the presence of nanoparticles has been discussed by Ramesh et al. [8]. Mukhopadhyay [9] analyzed time-dependent Maxwell fluid flow induced by a stretching surface with heat source/sink. Three-dimensional flow of Maxwell fluid with chemical reaction has been discussed by Hayat et al. [10].

In biomedical, engineering and industrial applications, heat transfer is very important phenomenon. Fourier [11] was the first one who described the heat transfer mechanism. The main flaw in Fourier's model is that initial disturbance is immediately observed by the medium under consideration. In reality this could not be possible, so it is called "paradox of heat conduction". Cattaneo [12] introduced a modification of Fourier's model in which heat flux relaxation time appeared when the temperature gradient is applied. Further modification of the Maxwell–Cattaneo's model is carried out by Christov [13]. He incorporated a Lie derivative in terms of constant time derivative for the heat flux. Ciarletta and Straughan [14] present particular and systemic constancy questions with Cattaneo–Christov heat flux model. Han et al. [15] studied coupled flow and heat transfer of viscoelastic fluid. Tibullo and Zampoli [16] examined particular result for the incompressible heat conducting Cattaneo–Christov model. Analogous heat convection problems in a Darcy's porous medium have been investigated by Straughan [17]. Ramesh et al. [18] studied analysis of heat transfer phenomenon in magnetohydrodynamic Casson fluid flow through Cattaneo–Christov heat flux. Hayat et al. [19] examined influence of chemical reaction and Cattaneo–Christov heat flux in MHD Oldroyd-B fluid flow. Liu et al. [20] studied anomalous convection diffusion and wave coupling transport of cells on comb frame with fractional Cattaneo–Christov flux.

Homogeneous–heterogeneous reactions are involved in many chemically reacting systems, for example, in combustion, catalysis and biochemical systems. Homogeneous and heterogeneous reactions are correlated in very complex manner. In the presence of a catalyst, some of the reactions proceed very slowly or not at all. Some common applications of chemical reactions are in ceramics and polymer production, food processing, hydrometallurgical industry, fog formation and dispersion and many others. Merkin [21] examined the fluid flow under the influence of homogeneous–heterogeneous reactions. He studied the homogeneous reaction with the help of cubic catalysis and the heterogeneous reaction with a first-order procedure. Chaudhary and Merkin [22] studied viscous fluid flow with chemical reaction. Stagnation point flow toward a surface with homogeneous–heterogeneous reactions has been examined by Bachok et al. [23]. Kameswaran et al. [24] studied nanofluid flow past a permeable stretching sheet with homogeneous heterogeneous reactions. Flow of viscoelastic fluid toward a surface subject to homogeneous–heterogeneous reactions has been investigated by Khan and Pop [25]. MHD flow of nanofluid under the influence of homogeneous–heterogeneous reactions has been studied by Hayat et al. [26]. Effect of homogeneous heterogeneous reactions and Newtonian heating in the Stagnation point flow of nanotubes has been analyzed by Hayat et al. [27]. Influence of homogeneous–heterogeneous reactions in flow of Powell–Eyring fluid has been investigated by Hayat et al. [28].

This article explores unsteady three-dimensional flow of Maxwell fluid. Flow is induced by a stretching sheet with heat transfer through Cattaneo–Christov heat flux model. Effect of homogeneous–heterogeneous reactions is also taken into consideration. Convergent series solutions are obtained by homotopy analysis method (HAM) [29–35]. The behaviors of different parameters on the physical quantities have been examined graphically.

2 Problem formulation

Consider the unsteady three-dimensional flow of Maxwell fluid induced by a stretching sheet at $z = 0$. Sheet is stretched with velocities $u_w(x) = cx/(1-\alpha t)$ and $v_w(y) = \mathrm{d}y/(1-\alpha t)$ along the x- and y-directions, respectively. An incompressible fluid fills the porous space. Heat transfer analysis is carried out by considering Cattaneo–Christov heat flux model. Here T_w is constant temperature of the sheet, whereas T_∞ is the temperature away from the sheet such that $T_w > T_\infty$ (see Fig 1).

Homogeneous–heterogenous reactions of two chemical species A and B are also taken into account. Homogeneous reactions at cubic autocatalysis can be demonstrated as:

$$A + 2B \rightarrow 3B, \quad \text{rate} = k_c a b^2, \tag{1}$$

and the heterogenous reaction in first-order isothermal is

$$A \rightarrow B, \quad \text{rate} = k_s a. \tag{2}$$

Here k_c and k_s are the rate constants and a and b are the concentrations of the species A and B. The governing boundary layer flow equations are as follows:

$$\frac{\partial u}{\partial x} + \frac{\partial v}{\partial y} + \frac{\partial w}{\partial z} = 0, \tag{3}$$

$$\begin{aligned} &\frac{\partial u}{\partial t} + u\frac{\partial u}{\partial x} + v\frac{\partial u}{\partial y} + w\frac{\partial u}{\partial z} \\ &\quad = \nu\frac{\partial^2 u}{\partial z^2} - \lambda\left(\frac{\partial^2 u}{\partial t^2} + 2u\frac{\partial^2 u}{\partial x \partial t} + 2v\frac{\partial^2 u}{\partial y \partial t} + 2w\frac{\partial^2 u}{\partial z \partial t} + u^2\frac{\partial^2 u}{\partial x^2} + v^2\frac{\partial^2 u}{\partial y^2}\right. \\ &\qquad \left. + w^2\frac{\partial^2 u}{\partial z^2} + 2uv\frac{\partial^2 u}{\partial x \partial y} + 2vw\frac{\partial^2 u}{\partial y \partial z} + 2uw\frac{\partial^2 u}{\partial x \partial z}\right) - \frac{\nu}{\hat{k}}u, \end{aligned} \tag{4}$$

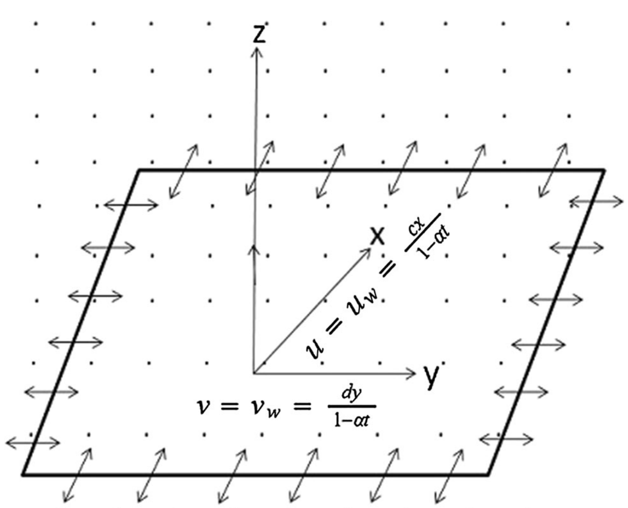

Fig. 1 Geometry of the problem

$$\begin{aligned} &\frac{\partial v}{\partial t} + u\frac{\partial v}{\partial x} + v\frac{\partial v}{\partial y} + w\frac{\partial v}{\partial z} \\ &\quad = \nu\frac{\partial^2 v}{\partial z^2} - \lambda\left(\frac{\partial^2 v}{\partial t^2} + 2u\frac{\partial^2 v}{\partial x \partial t} + 2v\frac{\partial^2 v}{\partial y \partial t} + 2w\frac{\partial^2 v}{\partial z \partial t} + u^2\frac{\partial^2 v}{\partial x^2} + v^2\frac{\partial^2 v}{\partial y^2}\right. \\ &\qquad \left. + w^2\frac{\partial^2 v}{\partial z^2} + 2uv\frac{\partial^2 v}{\partial x \partial y} + 2vw\frac{\partial^2 v}{\partial y \partial z} + 2uw\frac{\partial^2 v}{\partial x \partial z}\right) - \frac{\nu}{\hat{k}}v, \end{aligned} \tag{5}$$

$$\rho C_p\left(\frac{\partial T}{\partial t} + u\frac{\partial T}{\partial x} + v\frac{\partial T}{\partial y} + w\frac{\partial T}{\partial z}\right) = -\nabla.\mathbf{q}, \tag{6}$$

$$\frac{\partial a}{\partial t} + u\frac{\partial a}{\partial x} + v\frac{\partial a}{\partial y} + w\frac{\partial a}{\partial z} = D_A\frac{\partial^2 a}{\partial z^2} - k_c a b^2, \tag{7}$$

$$\frac{\partial b}{\partial t} + u\frac{\partial b}{\partial x} + v\frac{\partial b}{\partial y} + w\frac{\partial b}{\partial z} = D_B\frac{\partial^2 b}{\partial y^2} + k_c a b^2. \tag{8}$$

Corresponding boundary conditions are

$$\begin{aligned} &u = u_w = \frac{cx}{1-\alpha t}, \quad v = v_w = \frac{\mathrm{d}y}{1-\alpha t}, \quad w{=}0, \\ &\qquad T = T_w, \quad D_A\frac{\partial a}{\partial z} = k_s a, \quad D_B\frac{\partial b}{\partial z} = -k_s a \text{at} z = 0, \\ &u \rightarrow 0, \quad v \rightarrow 0, \quad T \rightarrow T_\infty, \quad a \rightarrow a_0, \quad b \rightarrow 0 \text{ as } z \rightarrow \infty, \end{aligned} \tag{9}$$

where the velocity components u , v and w are in the x-, y- and z-directions, respectively, μ the dynamic viscosity, ρ the density, λ the retardation time, $\hat{k}$ the permeability, C_p the specific heat, T the temperature, $\nu = \frac{\mu}{\rho}$ the kinematic viscosity of fluid, a_0 the positive dimensional constant, D_A and D_B the diffusion species coefficients of A and B and $\mathbf{q}$ the specific heat flux which satisfies [17]:

$$\mathbf{q} + \lambda_1\left(\frac{\partial \mathbf{q}}{\partial t} + \mathbf{V}.\nabla\mathbf{q} - \mathbf{q}.\nabla\mathbf{V} + (\nabla.\mathbf{V})\mathbf{q}\right) = -k\nabla T, \tag{10}$$

where k the fluid thermal conductivity and λ_1 is heat flux relaxation time. Here $\lambda_1 = 0$ corresponds to classical Fourier's law. As we know that fluid is incompressible so Eq. (10) becomes

$$\mathbf{q} + \lambda_1\left(\frac{\partial \mathbf{q}}{\partial t} + \mathbf{V}.\nabla\mathbf{q} - \mathbf{q}.\nabla\mathbf{V}\right) = -k\nabla T. \tag{11}$$

Eliminating $\mathbf{q}$ from Eqs. (6) and (11), we get

$$\frac{\partial T}{\partial t}+u\frac{\partial T}{\partial x}+v\frac{\partial T}{\partial y}+w\frac{\partial T}{\partial z}+\lambda_1\left(\frac{\partial^2 T}{\partial t^2}+2u\frac{\partial^2 T}{\partial x\partial t}+2v\frac{\partial^2 T}{\partial y\partial t}\right.$$
$$+2w\frac{\partial^2 T}{\partial z\partial t}+\frac{\partial u}{\partial t}\frac{\partial T}{\partial x}.+\frac{\partial v}{\partial t}\frac{\partial T}{\partial y}+\frac{\partial w}{\partial t}\frac{\partial T}{\partial z}+u^2\frac{\partial^2 T}{\partial x^2}+v^2\frac{\partial^2 T}{\partial y^2}$$
$$+w^2\frac{\partial^2 T}{\partial z^2}+u\frac{\partial u}{\partial x}\frac{\partial T}{\partial x}+u\frac{\partial v}{\partial x}\frac{\partial T}{\partial y}+u\frac{\partial w}{\partial x}\frac{\partial T}{\partial z}.$$
$$+v\frac{\partial u}{\partial y}\frac{\partial T}{\partial x}+v\frac{\partial v}{\partial y}\frac{\partial T}{\partial y}+v\frac{\partial w}{\partial z}\frac{\partial T}{\partial z}+w\frac{\partial u}{\partial z}\frac{\partial T}{\partial x}+w\frac{\partial v}{\partial z}\frac{\partial T}{\partial y}$$
$$+w\frac{\partial w}{\partial z}\frac{\partial T}{\partial z}+2uv\frac{\partial^2 T}{\partial x\partial y}.$$
$$\left.+2vw\frac{\partial^2 T}{\partial y\partial z}+2uw\frac{\partial^2 T}{\partial x\partial z}\right)=\frac{k}{\rho C_p}\left(\frac{\partial^2 T}{\partial x^2}+\frac{\partial^2 T}{\partial y^2}+\frac{\partial^2 T}{\partial z^2}\right). \tag{12}$$

Using transformations

$$\begin{gathered} u=\frac{cx}{1-\alpha t}r'(\xi),\quad v=\frac{cy}{1-\alpha t}s'(\xi), \\ w=\sqrt{\frac{cv}{1-\alpha t}}[r(\xi)+s(\xi)], \\ \theta(\xi)=\frac{T-T_\infty}{T_w-T_\infty},\quad \xi=\sqrt{\frac{c}{v(1-\alpha t)}}z, \\ a=a_0\phi(\xi),\quad b=a_0h(\xi). \end{gathered} \tag{13}$$

The continuity equation is satisfied accordingly and Eqs. (4), (5), (7–9) and (12) give:

$$\begin{aligned} &r'''-r'^2+(r+s)r''-A_1r'-\beta_1\big(r'''(r+s)^2-2r'r''(r+s)\\ &\quad-2A_1r''(r+s)+2A_1^2r'+2A_1r'^2\big)-k_1r'=0, \end{aligned} \tag{14}$$

$$\begin{aligned} &s'''-s'^2+(r+s)s''-A_1s'-\beta_1\big(s'''(r+s)^2-2s's''(r+s)\\ &\quad-2A_1s''(r+s)+2A_1^2s'+2A_1s'^2\big)-k_1s'=0, \end{aligned} \tag{15}$$

$$\begin{aligned} &\frac{1}{Pr}\theta''+(r+s)\theta'-\frac{1}{2}\xi A_1\theta'-\gamma\Big[(r+s)^2\theta''-A_1\xi(r+s)\theta''+\frac{1}{4}A_1^2\xi^2\theta''\\ &\quad+(r+s)(r'+s')\theta'-\frac{1}{2}A_1\xi(r'+s')\theta'-\frac{3}{2}A_1(r+s)\theta'+\frac{3}{4}A_1^2\xi\theta'\Big]=0, \end{aligned} \tag{16}$$

$$\frac{1}{Sc}\phi''+(r+s)\phi'-\frac{1}{2}A_1\xi\phi'-K\phi h^2=0, \tag{17}$$

$$\frac{\delta}{Sc}h''+(r+s)h'-\frac{1}{2}A_1\xi h'+K\phi h^2=0, \tag{18}$$

$$\begin{aligned} &r'(\xi)=1,\quad r(\xi)=0,\quad s'(\xi)=\beta_2,\quad s(\xi)=0,\\ &\quad\theta(\xi)=1\text{at}\xi=0,\\ &\phi'(\xi)=K_1\phi(\xi),\quad \delta h'(\xi)=-K_1\phi(\xi)\text{at}\xi=0,\\ &r'(\xi)\to 0,\quad s'(\xi)\to 0,\quad \theta(\xi)\to 0,\quad \phi(\xi)\to 1,\\ &\quad h(\xi)\to 0\text{ as }\xi\to\infty. \end{aligned} \tag{19}$$

Here prime denotes derivative with respect to ξ, $\beta_1=\frac{\lambda c}{1-\alpha t}$ is the Deborah number, $k_1=v(1-\alpha t)/\hat{k}c$ is the porosity parameter, $A_1=\frac{\alpha}{c}$ is the unsteady parameter,$Pr=v\rho C_p/k$ is the Prandtl number, $\gamma=\lambda_1c/(1-\alpha t)$ is the non-dimensional thermal relaxation parameter, $Sc=v/D_A$ is the Schmidt number, $K=k_ca_0^2(1-\alpha t)/c$ is the measure of the strength of the homogeneous reaction, $K_1=k_s\sqrt{v(1-\alpha t)}/D_A\sqrt{c}$ is the measure of the strength of the heterogeneous reaction, $\beta_2=d/c$ is the ratio of stretching rates and $\delta=D_B/D_A$ is the ratio of the diffusion coefficient.

Chemical species A and B having diffusion coefficients are assumed to be of approximate size. Further assuming that diffusion coefficients D_A and D_B are identical, i.e., $\delta=1$ [25]. Hence we have from Eq. (19)

$$\phi(\xi)+h(\xi)=1. \tag{20}$$

Thus Eqs. (17) and (18) become

$$\frac{1}{Sc}\phi''+(r+s)\phi'-\frac{1}{2}A_1\xi\phi'-K\phi(1-\phi)^2=0, \tag{21}$$

subject to the boundary conditions

$$\phi'(0)=K_1\phi(0),\quad \phi(\infty)\to 1. \tag{22}$$

Skin friction coefficients along the x- and y-directions are defined as follows:

$$C_{\mathrm{fx}}=\frac{\tau_{\mathrm{wx}}}{\rho u_w^2},\quad C_{\mathrm{fy}}=\frac{\tau_{\mathrm{wy}}}{\rho v_w^2}, \tag{23}$$

where the surface shear stresses τ_{wx} and τ_{wy} along the x- and y- directions are given by

$$\tau_{\mathrm{wx}}=\mu\left.\frac{\partial u}{\partial z}\right|_{z=0},\quad \tau_{\mathrm{wy}}=\mu\left.\frac{\partial v}{\partial z}\right|_{z=0}. \tag{24}$$

Dimensionless skin friction coefficients are

$$C_{\mathrm{fx}}(Re_x)^{1/2}=(1+\beta_1)f''(0),\quad C_{\mathrm{fy}}(Re_y)^{1/2}=(1+\beta_1)g''(0), \tag{25}$$

where $(Re_x)^{1/2}=x\sqrt{c/v}$ and $(Re_y)^{1/2}=y\sqrt{c/v}$ denote the local Reynolds number.

3 HAM solutions

The initial guesses and auxiliary operators are taken as follows:

$$\begin{gathered} r_0(\xi)=1-e^{-\xi},\quad s_0(\xi)=1-e^{-\xi},\quad \theta_0(\xi)=e^{-\xi},\\ \phi_0(\xi)=1-\frac{1}{2}e^{-K_1\xi}, \end{gathered} \tag{26}$$

$$\mathcal{L}_1 = r''' - r', \quad \mathcal{L}_2 = s''' - s', \quad \mathcal{L}_3 = \theta'' - \theta, \quad \mathcal{L}_4 = \phi'' - \phi, \tag{27}$$

with

$$\mathcal{L}_1(c_1 + c_2 e^{\xi} + c_3 e^{-\xi}) = 0, \quad \mathcal{L}_2(c_4 + c_5 e^{\xi} + c_6 e^{-\xi}) = 0, \quad \mathcal{L}_3(c_7 e^{\xi} + c_8 e^{-\xi}) = 0, \quad \mathcal{L}_4(c_9 e^{\xi} + c_{10} e^{-\xi}) = 0, \tag{28}$$

in which $c_1 - c_{10}$ are the constants.

Zeroth-order deformation equations are:

$$(1-p)\mathcal{L}_1[\hat{r}(\xi,p) - r_0(\xi)] = p\hbar_r \mathcal{N}_1[\hat{r}(\xi,p), \hat{s}(\xi,p)], \tag{29}$$

$$(1-p)\mathcal{L}_2[\hat{s}(\xi,p) - s_0(\xi)] = p\hbar_s \mathcal{N}_2[\hat{r}(\xi,p), \hat{s}(\xi,p)], \tag{30}$$

$$(1-p)\mathcal{L}_3\left[\hat{\theta}(\xi,p) - \theta_0(\xi)\right] = p\hbar_\theta \mathcal{N}_3[\hat{\theta}(\xi,p), \hat{r}(\xi,p), \hat{s}(\xi,p)], \tag{31}$$

$$(1-p)\mathcal{L}_4\left[\hat{\phi}(\xi,p) - \phi_0(\xi)\right] = p\hbar_\phi \mathcal{N}_4[\hat{\phi}(\xi,p), \hat{r}(\xi,p), \hat{s}(\xi,p)], \tag{32}$$

where $p \in [0,1]$ is the embedding parameter, $\mathcal{N}_1$, $\mathcal{N}_2$, $\mathcal{N}_3$ and $\mathcal{N}_4$ are the nonlinear operators and $\hbar_r$, $\hbar_s$, $\hbar_\theta$ and $\hbar_\phi$ are the nonzero auxiliary parameters. The nonlinear operators are

$$\begin{aligned}\mathcal{N}_1[\hat{r}(\xi,p), \hat{s}(\xi,p)] = {} & \frac{\partial^3 \hat{r}(\xi,p)}{\partial \xi^3} - \left(\frac{\partial \hat{r}(\xi,p)}{\partial \xi}\right)^2 \\ & + (\hat{r}(\xi,p) + \hat{s}(\xi,p))\frac{\partial^2 \hat{r}(\xi,p)}{\partial \xi^2} - A_1 \frac{\partial \hat{r}(\xi,p)}{\partial \xi} \\ & - \beta_1\Bigg((\hat{r}(\xi,p) + \hat{s}(\xi,p))^2 \frac{\partial^3 \hat{r}(\xi,p)}{\partial \xi^3} \\ & - 2(\hat{r}(\xi,p) + \hat{s}(\xi,p))\frac{\partial \hat{r}(\xi,p)}{\partial \xi}\frac{\partial^2 \hat{r}(\xi,p)}{\partial \xi^2}. \\ & - 2A_1 \frac{\partial^2 \hat{r}(\xi,p)}{\partial \xi^2}(\hat{r}(\xi,p) + \hat{s}(\xi,p)) \\ & + 2A_1^2 \frac{\partial \hat{r}(\xi,p)}{\partial v} + 2A_1\left(\frac{\partial \hat{r}(\xi,p)}{\partial \xi}\right)^2 \Bigg) \\ & - k_1 \frac{\partial \hat{r}(\xi,p)}{\partial \xi},\end{aligned} \tag{33}$$

$$\begin{aligned}\mathcal{N}_2[\hat{r}(\xi,p), \hat{s}(\xi,p)] = {} & \frac{\partial^3 \hat{s}(\xi,p)}{\partial \xi^3} - \left(\frac{\partial \hat{s}(\xi,p)}{\partial \xi}\right)^2 + (\hat{r}(\xi,p) \\ & + \hat{s}(\xi,p))\frac{\partial^2 \hat{s}(\xi,p)}{\partial \xi^2} - A_1 \frac{\partial \hat{s}(\xi,p)}{\partial \xi} \\ & - \beta_1\Bigg((\hat{r}(\xi,p) + \hat{s}(\xi,p))^2 \frac{\partial^3 \hat{s}(\xi,p)}{\partial \xi^3} \\ & - 2(\hat{r}(\xi,p) + \hat{s}(\xi,p))\frac{\partial \hat{s}(\xi,p)}{\partial \xi}\frac{\partial^2 \hat{s}(\xi,p)}{\partial \xi^2}. \\ & - 2A_1 \frac{\partial^2 \hat{s}(\xi,p)}{\partial \xi^2}(\hat{r}(\xi,p) + \hat{s}(\xi,p)) \\ & + 2A_1^2 \frac{\partial \hat{s}(\xi,p)}{\partial \xi} + 2A_1\left(\frac{\partial \hat{s}(\xi,p)}{\partial \xi}\right)^2 \Bigg) \\ & - k_1 \frac{\partial \hat{s}(\xi,p)}{\partial \xi},\end{aligned} \tag{34}$$

$$\begin{aligned}& \mathcal{N}_3\left[\hat{\theta}(\xi,p), \hat{r}(\xi,p), \hat{s}(\xi,p)\right] \\ & = \frac{1}{Pr}\frac{\partial^2 \hat{\theta}(\xi,p)}{\partial \xi^2} + (\hat{r}(\xi,p) + \hat{s}(\xi,p))\frac{\partial \hat{\theta}(\xi,p)}{\partial \xi} - \frac{1}{2}\eta A_1 \frac{\partial \hat{\theta}(\xi,p)}{\partial \xi} \\ & - \gamma\Bigg((\hat{r}(\xi,p) + \hat{s}(\xi,p))^2 \frac{\partial^2 \hat{\theta}(\xi,p)}{\partial \xi^2} - A_1 \xi (\hat{r}(\xi,p) + \hat{s}(\xi,p)) \\ & \frac{\partial^2 \hat{\theta}(\xi,p)}{\partial \xi^2} + \frac{1}{4}A_1^2 \xi^2 \frac{\partial^2 \hat{\theta}(\xi,p)}{\partial \xi^2} + (\hat{r}(\xi,p) + \hat{s}(\xi,p))\left(\frac{\partial \hat{r}(\xi,p)}{\partial \xi}\right. \\ & \left. + \frac{\partial \hat{s}(\xi,p)}{\partial \xi}\right)\frac{\partial \hat{\theta}(\xi,p)}{\partial \xi} - \frac{1}{2}A_1 \xi \left(\frac{\partial \hat{r}(\xi,p)}{\partial \xi} + \frac{\partial \hat{s}(\xi,p)}{\partial \xi}\right)\frac{\partial \hat{\theta}(\xi,p)}{\partial \xi} \\ & - \frac{3}{2}A_1(\hat{r}(\xi,p) + \hat{s}(\xi,p))\frac{\partial \hat{\theta}(\xi,p)}{\partial \xi} + \frac{3}{4}A_1^2 \xi \frac{\partial \hat{\theta}(\xi,p)}{\partial \xi}\Bigg),\end{aligned} \tag{35}$$

$$\begin{aligned}\mathcal{N}_4[\hat{\phi}(\xi,p), \hat{r}(\xi,p), \hat{s}(\xi,p)] = {} & \frac{1}{Sc}\frac{\partial^2 \hat{\phi}(\xi,p)}{\partial \xi^2} \\ & + (\hat{r}(\xi,p) + \hat{s}(\xi,p))\frac{\partial \hat{\phi}(\xi,p)}{\partial \xi} - \frac{1}{2}A_1 \xi \frac{\partial \hat{\phi}(\xi,p)}{\partial \xi} \\ & - k\hat{\phi}(\xi,p) - k\left(\hat{\phi}(\xi,p)\right)^3 + 2k(\hat{\phi}(\xi,p))^2,\end{aligned} \tag{36}$$

with boundary conditions

$$\hat{r}'(0,p) = 1, \quad \hat{r}(0,p) = 0, \quad \hat{r}'(\infty,p) = 0, \tag{37}$$

$$\hat{s}'(0,p) = \beta_2, \quad \hat{s}(0,p) = 0, \quad \hat{s}'(\infty,p) = 0, \tag{38}$$

$$\hat{\theta}(0,p) = 1, \quad \hat{\theta}(\infty,p) = 0, \tag{39}$$

$$\hat{\phi}'(0,p) = K_1 \hat{\phi}(0,p), \quad \hat{\phi}(\infty,p) = 1. \tag{40}$$

The mth-order deformation equations are

$$\mathcal{L}_1[r_m(\xi) - \chi_m r_{m-1}(\xi)] = \hbar_r \mathcal{R}_{r,m}(\xi), \tag{41}$$

$$\mathcal{L}_2[s_m(\xi) - \chi_m s_{m-1}(\xi)] = \hbar_s \mathcal{R}_{s,m}(\xi), \tag{42}$$

$$\mathcal{L}_3[\theta_m(\xi) - \chi_m\theta_{m-1}(\xi)] = \hbar_\theta \mathcal{R}_{\theta,m}(\xi), \tag{43}$$

$$\mathcal{L}_4[\phi_m(\xi) - \chi_m\phi_{m-1}(\xi)] = \hbar_\phi \mathcal{R}_{\phi,m}(\xi), \tag{44}$$

with

$$\chi_m = \begin{cases} 0, & m \leq 1 \\ 1, & m > 1 \end{cases}, \tag{45}$$

$$\begin{aligned}\mathcal{R}_{r,m}(\xi) = {} & r'''_{m-1} + \sum_{k=0}^{m-1}\left[r_{m-1-k}r''_k + s_{m-1-k}r''_k - r'_{m-1-k}r'_k\right] \\ & - A_1 r'_{m-1} - \beta_1\left(\sum_{l=0}^{m-1} r'''_{m-1-l}\left(\sum_{j=0}^{l} r_{l-j}r_j \right.\right. \\ & \left. + \sum_{j=0}^{l} s_{l-j}s_j + 2\sum_{j=0}^{l} r_{l-j}s_j\right) \\ & - \sum_{l=0}^{m-1} r''_{m-1-l}\left(2\sum_{j=0}^{l} r'_{l-j}r_j + 2\sum_{j=0}^{l} r'_{l-j}s_j\right) + 2A_1^2 r'_{m-1} \\ & \left. - 2A_1\sum_{k=0}^{m-1}[r''_{m-1-k}r_k - r''_{m-1-k}s_k] + 2A_1\sum_{k=0}^{m-1} r'_{m-1-k}r'_k\right) \\ & - k_1 r'_{m-1},\end{aligned} \tag{46}$$

$$\begin{aligned}\mathcal{R}_{s,m}(\xi) = {} & s'''_{m-1} + \sum_{k=0}^{m-1}\left[r_{m-1-k}s''_k + s_{m-1-k}s''_k - s'_{m-1-k}s'_k\right] \\ & - A_1 s'_{m-1} - \beta_1\left(\sum_{l=0}^{m-1} s'''_{m-1-l}\left(\sum_{j=0}^{l} r_{l-j}r_j \right.\right. \\ & \left. + \sum_{j=0}^{l} s_{l-j}s_j + 2\sum_{j=0}^{l} r_{l-j}s_j\right) \\ & - \sum_{l=0}^{m-1} s''_{m-1-l}\left(2\sum_{j=0}^{l} r_{l-j}s'_j + 2\sum_{j=0}^{l} s_{l-j}s'_j\right) + 2A_1^2 s'_{m-1} \\ & \left. - 2A_1\sum_{k=0}^{m-1}[s''_{m-1-k}r_k - s''_{m-1-k}s_k] + 2A_1\sum_{k=0}^{m-1} s'_{m-1-k}s'_k\right) \\ & - k_1 s'_{m-1},\end{aligned} \tag{47}$$

$$\begin{aligned}\mathcal{R}_{\theta,m}(\xi) = {} & \frac{1}{Pr}\theta''_{m-1} - \frac{1}{2}A_1\xi\theta'_{m-1} \\ & + \sum_{l=0}^{m-1}\left(\theta'_{m-1-l}r_l + \theta'_{m-1-l}s_l\right) \\ & - \gamma\left[\theta''_{m-1-l}\sum_{j=0}^{l}[r_{l-j}r_j + s_{l-j}s_j + 2r_{l-j}s_j]\right. \\ & + \theta'_{m-1-l}\sum_{j=0}^{l}[r_{l-j}r'_j + s_{l-j}s'_j + r_{l-j}s'_j + s_{l-j}r'_j] \\ & - A_1\xi\theta''_{m-1-l}r_l - A_1\xi\theta''_{m-1-l}s_l - \frac{1}{2}A_1\xi\theta'_{m-1-l}r_l \\ & \left. - \frac{1}{2}A_1\xi\theta'_{m-1-l}s_l - \frac{3}{2}A_1\theta'_{m-1-l}r_l - \frac{3}{2}A_1\theta'_{m-1-l}s_l\right],\end{aligned} \tag{48}$$

$$\begin{aligned}\mathcal{R}_{\phi,m}(\xi) = {} & \frac{1}{Sc}\phi''_{m-1} - \frac{1}{2}A_1\xi\phi'_{m-1} \\ & + \sum_{l=0}^{m-1}\left[\phi'_{m-1-l}r_l + \phi'_{m-1-l}s_l - K\phi_{m-1-l}\right. \\ & \left.\sum_{j=0}^{l}\phi_{l-j}\phi_j + 2k\phi_{m-1-l}\phi_l\right] - K\phi_{m-1}\end{aligned} \tag{49}$$

and the boundary conditions

$$\begin{aligned}& r'_m(0) = r_m(0) = r'_m(\infty) = s'_m(0) = s_m(0) = s'_m(\infty) = 0 \\ & \theta_m(0) = \theta_m(\infty) = \phi'_m(0) - K_s\phi_m(0) = \phi_m(\infty) = 0.\end{aligned} \tag{50}$$

The general solutions (r_m, s_m, θ_m, ϕ_m) comprising the special solutions (r^*_m, s^*_m, θ^*_m, ϕ^*_m) are given by

$$\begin{aligned}& r_m(\xi) = r^*_m(\xi) + c_1 + c_2e^{\xi} + c_3e^{-\xi}, \\ & s_m(\xi) = s^*_m(\xi) + c_4 + c_5e^{\xi} + c_6e^{-\xi}, \\ & \theta_m(\xi) = \theta^*_m(\xi) + c_7e^{\xi} + c_8e^{-\xi}, \\ & \phi_m(\xi) = \phi^*_m(\xi) + c_9e^{\xi} + c_{10}e^{-\xi},\end{aligned} \tag{51}$$

where the constants c_i ($i = 1, 2, \ldots, 10$) with the boundary conditions (50) are

$$\begin{aligned}& c_2 = c_5 = c_7 = c_9 = 0, \quad c_3 = \frac{\partial r^*_m(\xi)}{\partial\xi}\Big|_{\xi=0}, \quad c_6 = \frac{\partial s^*_m(\xi)}{\partial\xi}\Big|_{\xi=0}, \\ & c_1 = -c_3 - r^*_m(0), \quad c_4 = -c_6 - s^*_m(0), \quad c_8 = -\theta^*_m(0), \\ & c_{10} = \frac{1}{1+K_1}\left(\frac{\partial\phi^*_m(\xi)}{\partial\xi}\Big|_{\xi=0} - K_1\phi^*_m(0)\right).\end{aligned} \tag{52}$$

4 Convergence analysis

Homotopy analysis method gives us great choice to obtain the convergence of the series solutions. Region of convergence is controlled by auxiliary parameters $\hbar_r$, $\hbar_s$, $\hbar_\theta$ and $\hbar_\phi$. The admissible ranges of these parameters are $-0.9 \leq \hbar_r \leq -0.5$, $-1.0 \leq \hbar_s \leq -0.4$, $-1.4 \leq \hbar_\theta \leq -0.6$ and $-0.8 \leq \hbar_\phi \leq -0.4$ (Figs. 2, 3, 4, 5).

Table 1 gives the convergence of series solutions of velocities, temperature and concentration distributions.

5 Results and discussion

5.1 Dimensionless velocity profiles

Here we discuss the impact of different embedded parameters on dimensionless velocity profiles r' and s'. Figure 6 depicts the variation of Deborah number β_1 on velocity profiles. As viscous forces are dominant for larger Deborah number which resist the fluid motion, so fluid flows along the x- and y-directions. Figure 7 shows the impact of ratio of stretching rates β_2 on velocity profiles. Increasing values of β_2 shows higher rate of stretching. When we increase the ratio of stretching rates, the velocity along x-direction decreases, while the velocity along y-direction increases. Figure 8 presents the velocity profiles for larger value of porosity parameter k_1. Here velocity profiles are decreasing functions of k_1. As increasing porosity parameter causes a decrease in permeability of fluid which reduces the fluid flow. Impact of unsteady parameter A_1 on velocity field is shown in Fig. 9. When unsteady parameter A_1 increases, the stretching constant decreases hence velocity decreases.

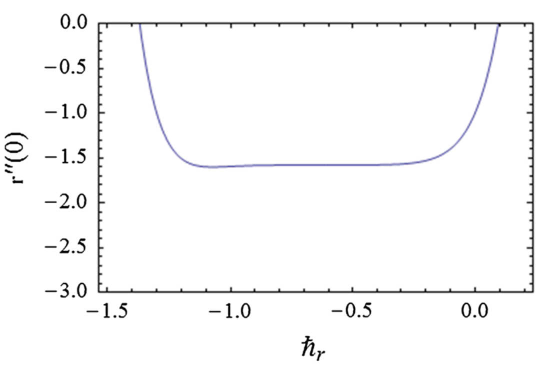

Fig. 2 $\hbar$-curve for $r''(0)$

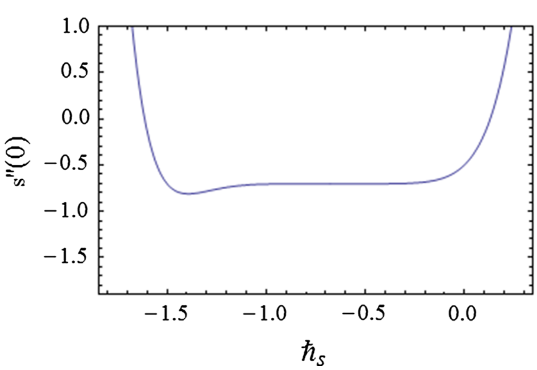

Fig. 3 $\hbar$-curve for $s''(0)$

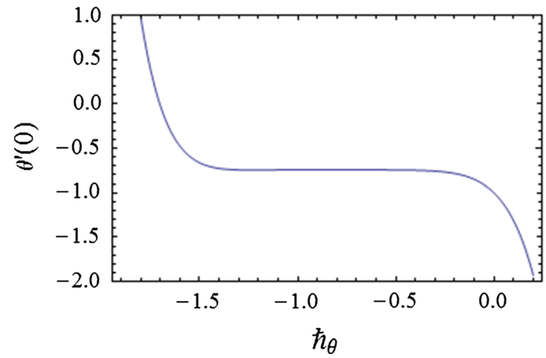

Fig. 4 $\hbar$-curve for $\theta'(0)$

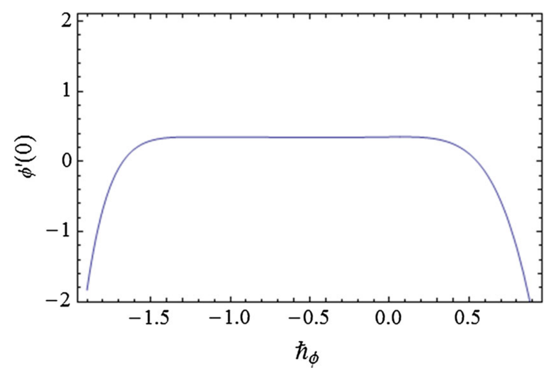

Fig. 5 $\hbar$-curve for $\phi'(0)$

Table 1 Convergence of series solutions when $A_1 = 0.1$, $\gamma = 1.0$, $\beta_1 = 0.5$, $\beta_2 = 0.5$, $K = 0.2$, $Pr = 1.0$, $Sc = 1.4$, $k_1 = 0.6$ and $K_1 = 0.7$

Order of approximation	$r''(0)$	$s''(0)$	$\theta'(0)$	$\phi'(0)$
1	− 1.429	− 0.6409	− 0.8806	0.3931
5	− 1.580	− 0.7045	− 0.7459	0.3761
7	− 1.582	− 0.7053	− 0.7394	0.3738
8	− 1.582	− 0.7054	− 0.7390	0.3732
13	− 1.582	− 0.7054	− 0.7408	0.3723
17	− 1.582	− 0.7054	− 0.7415	0.3721
19	− 1.582	− 0.7054	− 0.7416	0.3721
30	− 1.582	− 0.7054	− 0.7416	0.3721
37	− 1.582	− 0.7054	− 0.7416	0.3721
45	− 1.582	− 0.7054	− 0.7416	0.3721

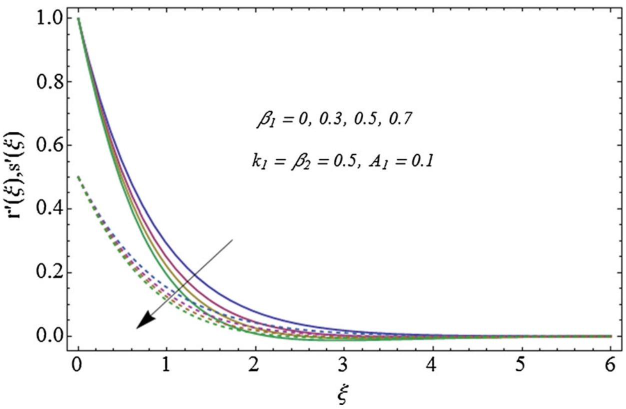

Fig. 6 Behavior of β_1 on $r'(\xi)$ and $s'(\xi)$

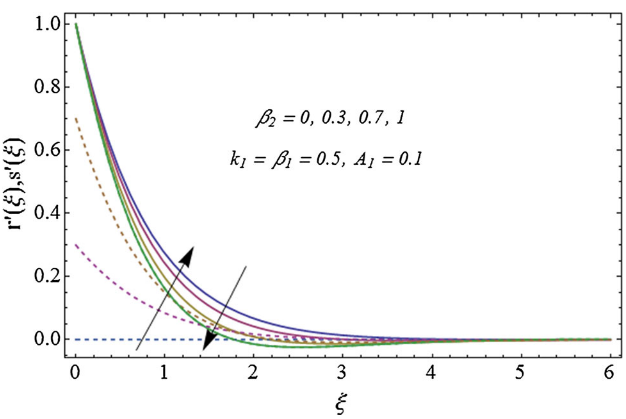

Fig. 7 Behavior of β_2 on $r'(\xi)$ and $s'(\xi)$

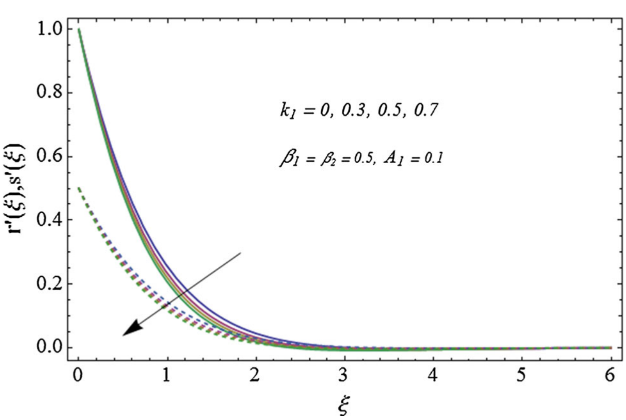

Fig. 8 Behavior of k_1 on $r'(\xi)$ and $s'(\xi)$

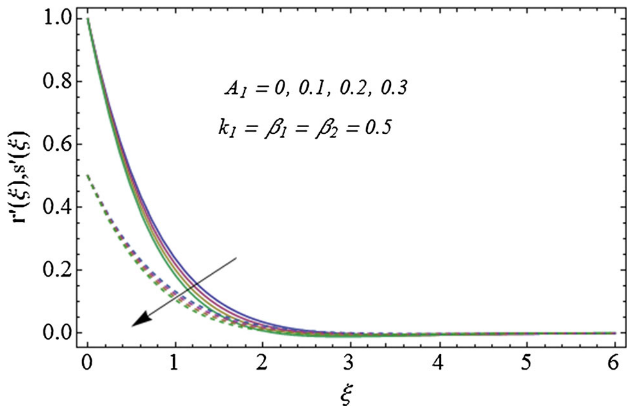

Fig. 9 Behavior of A_1 on $r'(\xi)$ and $s'(\xi)$

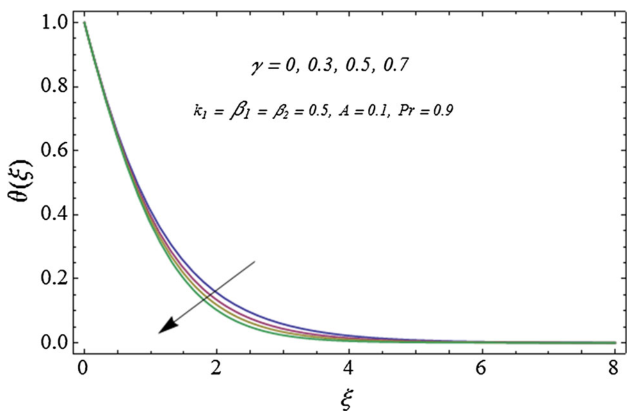

Fig. 10 Behavior of γ on $\theta(\xi)$

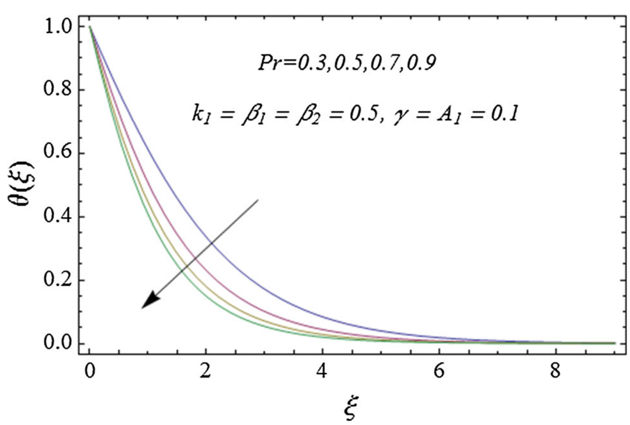

Fig. 11 Behavior of Pr on $\theta(\xi)$

5.2 Dimensionless temperature profile

Now we discuss the behavior of involved parameters on dimensionless temperature profile $\theta(\xi)$. Impact of thermal relaxation time γ on temperature field is illustrated in Fig. 10. Temperature profile decreases for increasing thermal relaxation time. Because particles show non-conducting behavior when thermal relaxation time is increased, i.e., particles need more time to transfer heat so the temperature decreases. Figure 11 shows the variation of Prandtl number Pr on temperature profile. As thermal diffusivity decreases, when the Prandtl number is enhanced; hence, the temperature profile decreases.

5.3 Dimensionless concentration profile

Figures 12, 13, 14 and 15 show the behavior of Schmidt number Sc, the measure of strength of the homogeneous reactions K, the measure of strength of the heterogeneous reaction K and the ratio of stretching rates β_2 on concentration profile $\phi(\xi)$. Figure 12 depicts impact of Sc on $\phi(\xi)$. Larger values of Schmidt number correspond to an increase in concentration profile. Ratio of momentum to mass diffusion rate is known as Schmidt number. For higher Schmidt number, the momentum diffusion rate increases and consequently concentration field enhances. Figure 13 shows there is decrease in concentration field when homogeneous reaction parameter K increases. This is because during homogeneous reaction the reactants are consumed. Figure 14 depicts that concentration profile enhances when we increase the heterogeneous reaction parameter K_1. Figure 15 illustrates the behavior of β_2 on $\phi(\xi)$. Here larger β_2 enhances the concentration field increases. This is because of decreased stretching rate in x-direction.

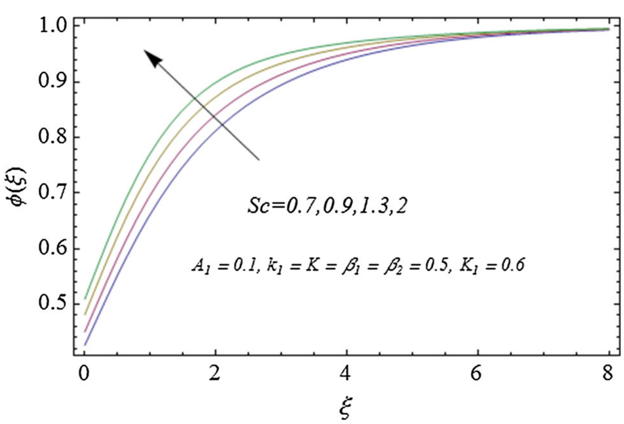

Fig. 12 Behavior of Sc on $\phi(\xi)$

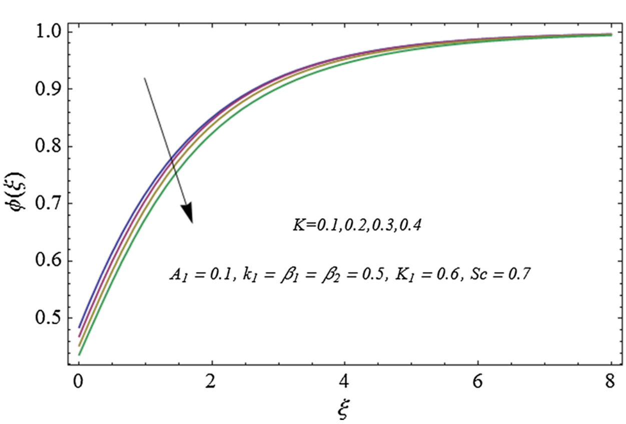

Fig. 13 Behavior of K on $\phi(\xi)$

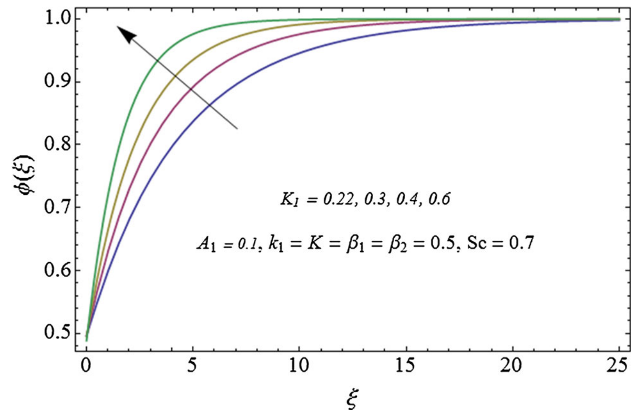

Fig. 14 Behavior of K_1 on $\phi(\xi)$

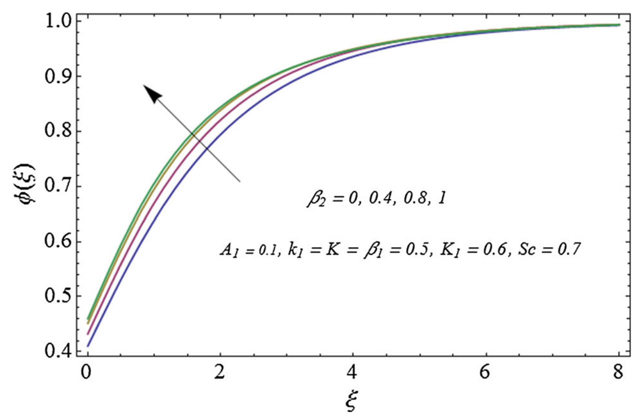

Fig. 15 Behavior of β_2 on $\phi(0)$

5.4 Surface concentration

Effects of homogeneous reaction parameter K and heterogeneous reaction parameter K_1 on surface concentration $\phi(0)$ are shown in the Figs. 16 and 17. From Fig. 16, we observe that $\phi(0)$ decreases when we increase the strength of homogeneous reaction K. Figure 17 shows that surface concentration enhances for larger strength of

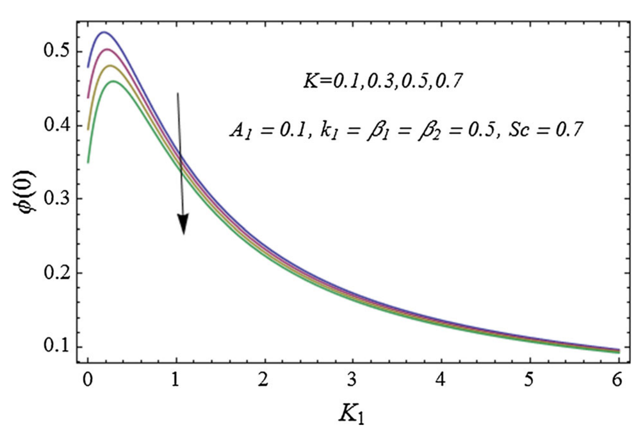

Fig. 16 Behavior of K on $\phi(0)$

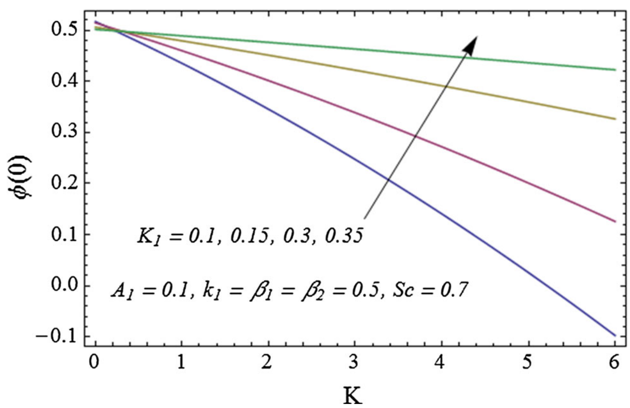

Fig. 17 Behavior of K_1 on $\phi(0)$

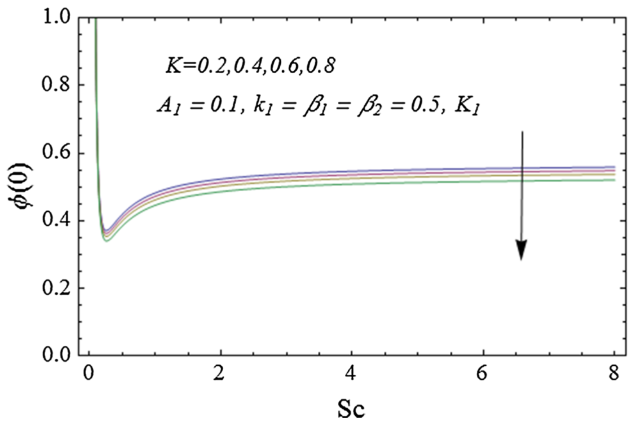

Fig. 18 Behavior of K on $\phi(0)$

Table 2 Values of $-f''(0)$ for various values of Deborah number β_1 when $A_1 = k_1 = 0$

β_1	Mukhopadhyay [9]	Hayat et al. [10]	Present results
0	0.999963	0.999962	0.99996
0.2	1.051949	1.051948	1.05195
0.4	1.101851	1.101850	1.10185
0.6	1.150162	1.150160	1.15016
0.8	1.196693	1.196694	1.19669

heterogeneous reaction parameter K_1. Figure 18 depicts behavior of homogeneous reaction parameter K via Schmidt number Sc on surface concentration $\phi(0)$. Here $\phi(0)$ decreases when K is increased.

Table 2 shows the comparison of the present results with the numerical solution of Mukhopadhyay [9] and Hayat et al. [10] in limiting case. It is found that our solution has good agreement with the limiting numerical solution.

6 Main results

Cattaneo–Christov heat flux model is used to examine time-dependent flow of Maxwell fluid with chemical reaction. Main points are given below:

- Velocity profiles are decreasing functions of Deborah number, porosity parameter and unsteady parameter.
- Temperature is decreasing function of thermal relaxation time and Prandtl number.
- Concentration profile increases for larger Schmidt number and it decreases for when homogeneous reaction parameter increases.
- Impact of strengths of homogeneous and heterogeneous reactions is opposite on wall concentration.
- Present problem has many applications like food processing, clay coatings, hydrometallurgical industry, fog formation and dispersion.

Compliance with ethical standards

Conflict of interest The authors confirm that this article content has no conflict of interest.

References

1. Sui J, Zheng L, Zhang X (2016) Boundary layer heat and mass transfer with Cattaneo–Christov double-diffusion in upper-convected Maxwell nanofluid past a stretching sheet with slip velocity. Int J Therm Sci 104:461–468
2. Jamil M, Fetecau C (2010) Helical flows of Maxwell fluid between coaxial cylinders with given shear stresses on the boundary. Commun Nonlinear Sci Numer Simul 15:3931–3938
3. Wang S, Tan W (2011) Stability analysis of soret-driven double-diffusive convection of Maxwell fluid in a porous medium. Int J Heat Fluid Flow 32:88–94
4. Abbasbandy S, Naz R, Hayat T, Alsaedi A (2014) Numerical and analytical solutions for Falkner–Skan flow of MHD Maxwell fluid. Appl Math Comput 242(1):569–575
5. Awais M, Hayat T, Alsaedi A, Asghar S (2014) Time-dependent three-dimensional boundary layer flow of a Maxwell fluid. Comput Fluids 91:21–27
6. Ramesh GK, Gireesha BJ (2014) Influence of heat source/sink on a Maxwell fluid over a stretching surface with convective boundary condition in the presence of nanoparticles. Ain Shams Eng 5:991–998
7. Ramesh GK, Prasannakumara BC, Gireesha BJ, Shehzad SA, Abbasi FM (2017) Three dimensional flow of Maxwell fluid with suspended nanoparticles past a bidirectional porous stretching surface with thermal radiation. Therm Sci Eng Prog 1:6–14
8. Ramesh GK, Gireesha BJ, Hayat T, Alsaedi A (2016) Stagnation point flow of Maxwell fluid towards a permeable surface in the presence of nanoparticles. Alex Eng J 55:857–865
9. Mukhopadhyay S (2012) Heat transfer analysis of the unsteady flow of a Maxwell fluid over a stretching surface in the presence of a heat source/sink. Chin Phys Lett 29:054703

10. Hayat T, Imtaiz M, Almezal S (2015) Modeling and analysis for three dimensional flow with homogeneous–heterogeneous reactions. AIP Adv 5:107209
11. Fourier JBJ (1822) Theorie analytique De La chaleur (Paris, 1822)
12. Cattaneo C (1948) Sulla conduzione del calore. Atti Semin Mat Fis Uni Modena Reggio Emilia 3:83–101
13. Christov CI (2009) On frame indifferent formulation of the Maxwell–Cattaneo model of finite-speed heat conduction. Mech Res Commun 36:481–486
14. Ciarletta M, Straughan B (2010) Uniqueness and structural stability for the Cattaneo–Christov equations. Mech Res Commun 37:445–447
15. Han S, Zheng L, Li C, Zhang X (2014) Coupled flow and heat transfer in viscoelastic fluid with Cattaneo–Christov heat flux model. Appl Math Lett 38:87–93
16. Tibullo V, Zampoli V (2011) A uniqueness result for the Cattaneo–Christov heat conduction model applied to incompressible fluids. Mech Res Commun 38:77–79
17. Straughan B (2010) Porous convection with Cattaneo heat flux. Int J Heat Mass Transf 53:2808–2812
18. Ramesh GK, Gireesha BJ, Shehzad SA, Abbasi FM (2017) Analysis of heat transfer phenomenon in magnetohydrodynamic Casson fluid flow through Cattaneo–Christov heat diffusion theory. Commun Theor Phys 68:91–95
19. Hayat T, Imtiaz M, Alsaedi A, Almezal S (2016) On Cattaneo–Christov heat flux in MHD flow of Oldroyd-B fluid with homogeneous–heterogeneous reactions. J Magn Magn Mater 401:296–303
20. Liu L, Zheng L, Liu F, Zhang X (2016) Anomalous convection diffusion and wave coupling transport of cells on comb frame with fractional Cattaneo–Christov flux. Commun Nonlinear Sci Numer Simul 38:45–58
21. Merkin JH (1996) A model for isothermal homogeneous–heterogeneous reactions in boundary layer flow. Math Comput Model 24:125–136
22. Chaudhary MA, Merkin JH (1995) A simple isothermal model for homogeneous-heterogeneous reactions in boundary layer flow I. Equal diffusivities. Fluid Dyn Res 16:311–333
23. Bachok N, Ishak A, Pop I (2011) On the stagnation-point flow towards a stretching sheet with homogeneous–heterogeneous reactions effects. Commun Nonlinear Sci Numer Simul 16:4296–4302
24. Kameswaran PK, Shaw S, Sibanda P, Murthy PVSN (2013) Homogeneous–heterogeneous reactions in a nanofluid flow due to porous stretching sheet. Int J Heat Mass Transf 57:465–472
25. Khan WA, Pop I (2015) Effects of homogeneous–heterogeneous reactions on the viscoelastic fluid towards a stretching sheet. ASME J Heat Transf 134:064506
26. Hayat T, Imtiaz M, Alsaedi A (2015) MHD flow of nanofluid with homogeneous—heterogeneous reactions and velocity slip. Therm. Sci. https://doi.org/10.2298/TSCI140922067H
27. Hayat T, Farooq M, Alsaedi A (2015) Homogeneous–heterogeneous reactions in the stagnation point flow of carbon nanotubes with Newtonian heating. AIP Adv 5:027130
28. Hayat T, Imtiaz M, Alsaedi A (2015) Effects of homogeneous–heterogeneous reactions in flow of Powell–Eyring fluid. J Cent South Univ 22(8):3211–3216
29. Sui J, Zheng L, Zhang X, Chen G (2015) Mixed convection heat transfer in power law fluids over a moving conveyor along an inclined plate. Int J Heat Mass Transf 85:1023–1033
30. Farooq U, Zhao YL, Hayat T, Alsaedi A, Liao SJ (2015) Application of the HAM-based mathematica package BVPh 2.0 on MHD Falkner–Skan flow of nanofluid. Comput Fluids 111:69–75
31. Abbasbandy S, Yurusoy M, Gulluce H (2014) Analytical solutions of non-linear equations of power-law fluids of second grade over an infinite porous plate. Math Comput Appl 19(2):124
32. Hatami M, Nouri R, Ganji DD (2013) Forced convection analysis for MHD Al_2O_3-water nanofluid flow over a horizontal plate. J Mol Liq 187:294–301
33. Turkyilmazoglu M (2012) Solution of the Thomas–Fermi equation with a convergent approach. Commun Nonlinear Sci Numer Simul 17:4097–4103
34. Arqub OA, El-Ajou A (2013) Solution of the frictional epidemic model by homotopy analysis method. J King Saud Univ Sci 25:73–81
35. Ellahi R, Hassan M, Zeeshan A (2015) Shape effects of nanosize particles in Cu-H_2O nanofluid on entropy generation. Int J Heat Mass Transf 81:449–456